Steel and Composite Structures, *Vol. 22, No. 1 (2016) 141-159*
DOI: http://dx.doi.org/10.12989/scs.2016.22.1.141

Rotation capacity of composite beam connected to RHS column, experimental test results

Mohammadreza Eslami [1a] and Hisashi Namba [*2]

[1] *Department of Architecture, Kobe University, Japan*
[2] *Department of Architecture, Kobe University, 1-1 Rokkodai, Nada ku, Kobe, 657-8501, Japan*

(*Received August 31, 2015, Revised September 22, 2016, Accepted September 23, 2016*)

Abstract. Commonly in steel frames, steel beam and concrete slab are connected together by shear keys to work as a unit member which is called composite beam. When a composite beam is subjected to positive bending, flexural strength and stiffness of the beam can be increased due to "composite action". At the same time despite these advantages, composite action increases the strain at the beam bottom flange and it might affect beam plastic rotation capacity. This paper presents results of study on the rotation capacity of composite beam connected to Rectangular Hollow Section (RHS) column in the steel moment resisting frame buildings. Due to out-of-plane deformation of column flange, moment transfer efficiency of web connection is reduced and this results in reduction of beam plastic rotation capacity. In order to investigate the effects of width-to-thickness ratio (B/t) of RHS column on the rotation capacity of composite beam, cyclic loading tests were conducted on three full scale beam-to-column subassemblies. Detailed study on the different steel beam damages and concrete slab damages are presented. Experimental data showed the importance of this parameter of RHS column on the seismic behavior of composite beams. It is found that occurrence of severe concrete bearing crush at the face of RHS column of specimen with smaller width-to-thickness ratio resulted in considerable reduction on the rate of strain increase in the bottom flange. This behavior resulted in considerable improvement of rotation capacity of this specimen compared with composite and even bare steel beam connected to the RHS column with larger width-to-thickness ratio.

Keywords: composite beam; rectangular hollow section column; cyclic loading test; rotation capacity; connection factor

1. Introduction

In Japan following to the 1995 Hyogo ken-Nanbu (Kobe) earthquake, fractures occurred in the beam-to-column connections of a number of steel moment frame buildings (AIJ 1995d 1995 - Nakashima *et al*. 2002), which was similar to that extensively found in the 1994 U.S. Northridge earthquake (FEMA-355E 2000). According to post-earthquake observations in most cases fractures were happened at the bottom flanges and it is believed that composite action might be one of the reasons of such failure. Most of post-earthquake researches regarding the rotation capacity of beam were conducted on the bare steel beam specimens rather than composite specimens. According to past researches, it is already well known that in the case of an effective

*Corresponding author, Associate Professor, E-mail: namba@kobe-u.ac.jp
[a] Ph.D., E-mail: eslami@msu.edu

http://www.techno-press.org/?journal=scs&subpage=6 ISSN: 1229-9367 (Print), 1598-6233 (Online)

composite action of the slab, the neutral axis is shifted toward top flange and, for sagging moments, in case of such a typology of beam-to-column connections almost always the failure occurs in the bottom flange. This type of failure occurs due to strain concentration at the bottom flange, and reduces the rotation capacity of composite beam. However, the question arises that how strain is affected by different width-to-thickness ratios of RHS columns, and how strain condition changes after the occurrence of damages in the concrete slab? The objective of this research conducted in the Kobe University was to in investigate the effect of column's width-to-thickness ratio in the presence of concrete slab.

In the Japanese steel practice, application of Rectangular Hollow Section Column (*RHS*) in the Seismic Moment Resisting Frame buildings (*SMRF*) is dominant (Nakashima *et al*. 2002). In the case of beam-to-RHS column connection, beam flanges are usually connected to column by through diaphragms, while beam web is connected to RHS column wall (flange) directly without any reinforcement. This might cause local out-of-plane deformation of column flange at the web connection. In this condition full capacity of beam web cannot be transmitted. This effect has been investigated for the bare steel beam (AIJ 2012), however in the case of composite beam due to existence of concrete slab, web connection might be in more severe stress condition, shown in Fig. 1. According to the research conducted by Okada and Yamada (2001), plastic rotation capacity of composite beam connected to RHS column decreased to almost half of bare steel beam. Further Research by Okada *et al*. (2004) was conducted on the composite beams which were connected to the H-section (representing a RHS column which thickness of wall is infinite) and RHS columns with different width-to-thickness ratios of 24 and 38, and it was shown that significant reduction of composite beam rotation capacity will occur in the case of RHS column with large width-to-thickness ratios. Okada showed that out-of-plane deformation of RHS column is affected by reduction of web flexural capacity and movement of neutral axis toward beam top flange.

Matsuo *et al*. (2000) conducted experimental test focusing on the rotation capacity of composite beam connected to the RHS column with width-to-thickness ratio of 29. According to that test results, rotation capacity of composite beam specimens were almost half of bare steel beam specimens. However, in current structural design, rotation capacity of composite beam is supposed to be equal to the bare steel beam.

This research is aiming to understand the mechanical mechanism of out-of-plane deformation of RHS column and its effect on the behavior of composite beam. In most previous research

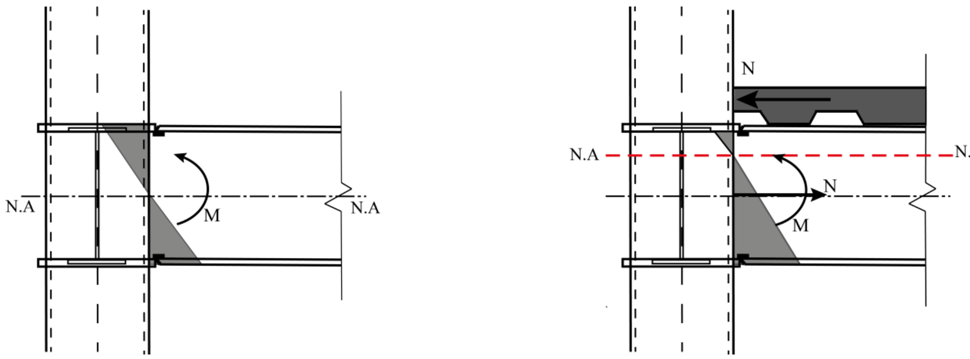

(a) Bare steel beam (b) Composite beam

Fig. 1 Strain concentration on bottom flange and severe condition of web out-of-plane deformation due to existence of slab in the positive flexure studies dealing with composite beam-to-box column connections, effect of out-of-plane deformation was taken in to consideration based on reduction of web flexural capacity approach (Kim and Oh 2007, Sanaei Nia *et al*. 2014, Yu *et al*. 2015). This research is conducted to clarify the structural condition of web connection, not only based on the flexural capacity considerations, but also by considering the effect of axial force subjected to the web. Since limited experimental test data with application of post-Kobe earthquake requirements for welding and design of connection is available, as the first part of this research program, actual behavior of composite beam connected to the RHS column with two different width-to-thickness ratios are studied through experimental tests. Results of different strength, stiffness and rotation capacity of beams are discussed through the study on the different damages in the steel beams and concrete slabs. Contribution of concrete slab on the condition of strain is investigated and strain studies before and after concrete crush were carried out to investigate the effects of bottom flange strain on the rotation capacity of composite beam.

2. Experimental test specification

2.1 Test specimens

In order to investigate the effects of RHS column width-to-thickness ratio on the rotation capacity of composite beam, cyclic loading test using T-shaped subassembly were conducted on three subassemblies of H-Beam (500×200×10×16) connected to RHS column with two different width-to-thickness ratios of 29 and 22 (□-350×350×12 & □-350×350×16). These two ratios were decided based on the common sections which are used in the actual construction of mid-rise buildings, and the principle of strong column-week beam is applied in the design of specimens. As shown in Table 1, one bare steel beam specimen and two composite beam specimens were prepared. Fig. 2 illustrates the configuration of specimens, test setups, weld joint details, steel deck geometry and column section, respectively. Lateral supports shown in this Figure, were prepared just for the safety in the test. Therefore, the hing which is predicted in the middle of these two members is to prevent the possiblity of sustaining load by the support.

As shown in the Fig. 2, concrete slab with width of 1500 mm and thickness of 80 mm were used for composite beam specimens. The concrete slab was provided with longitudinal and transverse steel reinforcement. In these specimens, deck plate type QL 99-50-12 applied according to Design Recommendations for Composite Constructions AIJ (2010), and two stud bolts of ϕ16 with height of 80 mm were welded to the beam flange with pitch distance of 300 mm. Transverse distance between studs was considered as 80 mm. The number of shear studs is common to all specimens. Deck plate geometry and detail of reinforcement is shown in Fig. 3. The nominal shear

Table 1 Specimens specification

Specimen	Concrete slab	RHS column width-to-thickness (B/t) ratio
BS-29	Not	29
CB-29	Existed	29
CB-22	Existed	22
Beam: H-500×200×10×16		Column: □-350×350×t

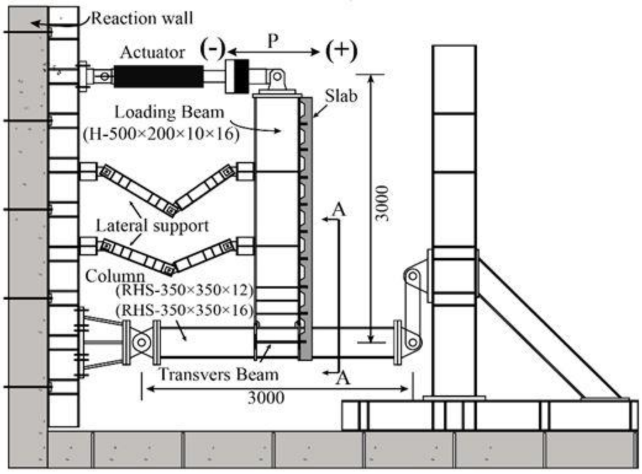

(a) Composite beam specimen and test setup

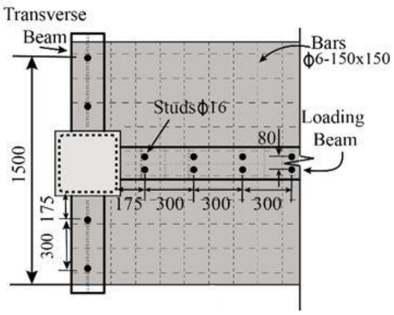

(b) Section A-A

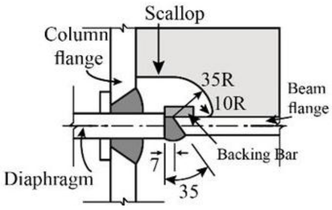

(c) Weld joint detail

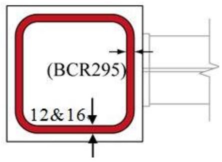

(e) Box column section
□-350×350×*t*

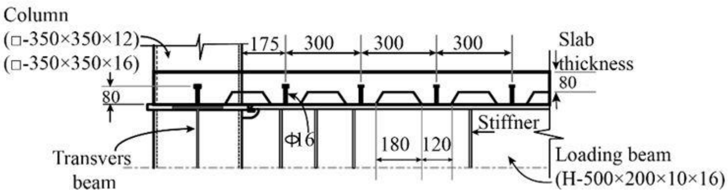

(d) Deck geometry

Fig. 2 Configuration of specimens and test setups

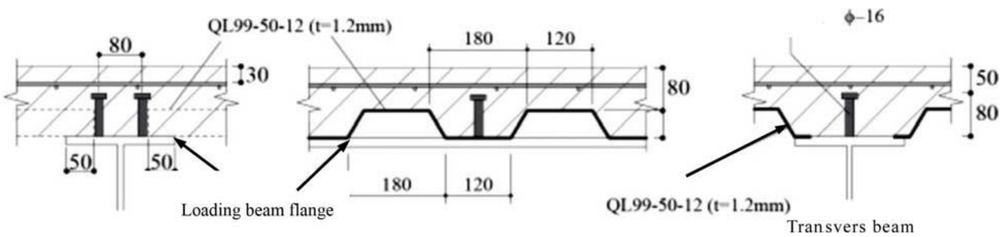

Fig. 3 Deck plate type QL 99-50-12 geometry and detail of reinforcement

force between the steel beam and the concrete slab transferred by studs, Q_h, shall be determined as the lowest value in accordance with the concrete crushing, or tensile yielding of the steel section (AIJ (2010) - AISC 360-10 (2010)). So, Design of studs in the specimen is conducted by considering the minimum of

$$Q_h = \min\left(C, {}_bF_y\right) \tag{1}$$

Where "C" is Effective compression strength of the concrete slab, "${}_bF_y$" is the tensile yield strength of steel section (equals to $\sigma_y A_s$). According to Design Recommendations for Composite Constructions AIJ (2010), the nominal shear strength of one stud q_s, shall be determined as follows

$$q_s = 0.5 \times {}_{sc}a \sqrt{f_c \cdot E_c} \tag{2}$$

Where "${}_{sc}a$" is cross-sectional area of the stud [mm^2], "E_c" is Concrete modulus of elasticity [N/mm^2], "f_c" is Concrete compressive strength [N/mm^2]. Concrete Young modulus is calculated by

$$E_c = 21000 \times \left(\frac{\gamma}{23}\right)^{1.5} \times \sqrt{\frac{f_c}{20}} \tag{3}$$

The required number of studs shall be equal to the horizontal shear divided by the nominal shear strength of one stud

$$n_r = Q_h / \; q_s \tag{4}$$

Fig. 4 shows the completed specimen before the start of loading.

Fig. 4 Picture of the completed composite specimen

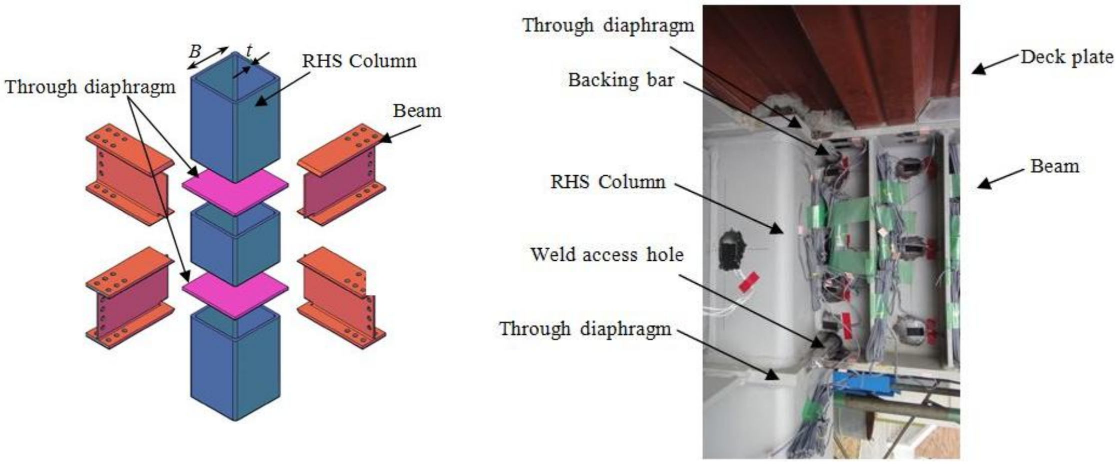

(a) Joint detail according to JASS 6 (2007) (b) Test specimen joint detail

Fig. 5 Joint detail for beam-to-box column connection

2.2 Weld Joint details

Weld Joint detail for beam-to-RHS column connection is illustrated in Figs. 2(c) and 5. According to the steel practice in Japan, beam flanges are connected to the column by "through diaphragm" to achieve smooth stress transfer from beam flange to the column, and preventing local deformation of RHS column wall. Beam web is connected to the wall of RHS column without reinforcement, and fillet welds were applied in both sides of the beam. This detail is common in Japan and it is recommended in JASS 6 2007 as an effective method (Yamada *et al*. 2009). In all specimens shop welded joint type used by complete joint penetration (CJP) groove welds. CO_2 gas shielded metal arc welding method (GMAW) using YGW11 electrodes was conducted. Ceramic run of tabs were used and backing bars left in place. The weld access hole which is known as "scallop", was consisted of two arcs with radiuses of 35 and 10 millimetres, which is corresponded to post Hyogo ken-Nanbu (Kobe) earthquake weld scallop geometry type (AIJ 2012).

2.3 Material properties

The material utilized for the specimens were hot rolled sections with steel grade of SM490A and cold formed BCR295 for beams and columns, respectively. Diaphragm plates material were used with steel grade SN 490B. Actual material properties obtained by tensile coupon tests are reported in Table 2.

Regarding the beam material toughness, Fig. 6(a) plots the values of material Charpy V-Notch (CVN) impact test results associated with "fillet" area, which obtained from coupon tests. Fillet area is defined as the meeting point between the web and the flange which is illustrated in Fig. 6(b).

Studs material were used with steel grade JIS B1198-1995 (Design Recommendations for Composite Constructions AIJ 2010), and push-out tests were also carried out for the purpose of evaluating the shear strength and elastic stiffness of shear studs, summarized in Table 3.

Table 2 Material properties

Member		Material grade	σ_y (N/mm^2)	σ_u (N/mm^2)	YR = σ_y/σ_u	EL (%)
Beam	Flange	SM490A	383	551	69.5	40.6
	Web		422	541	78.1	36.6
RHS column	CB-29	BCR295	328	425	77.0	48.9
	CB-22		369	471	78.3	43.4
Diaphragm		SN490B	370	531	69.7	49.9
Weld metal		YGW11	420	536	78.3	31.4

Table 3 Shear stud push out test results

Elastic stiffness (KN/mm)	Shear strength q_y (KN)	Ultimate shear strength $q_{\max}$ (KN)	$\delta_{\max}$ (mm)
346.9	65.5	88.9	2.36

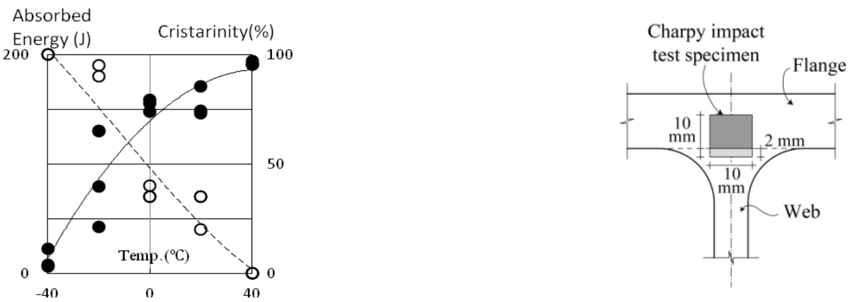

(a) CVN test results (b) Location of charpy impact test specimen

Fig. 6 Charpy V-Notch impact test results for "fillet" area of beam

The design strength of concrete used for composite beam specimens was 21.0 N/mm^2. The average concrete strength from cylinder tests was 28.4 N/mm^2 .

2.4 Test procedure

As shown in Fig. 2, specimens were simply supported at both ends of column and the lateral load was applied at the top of beam. The cyclic loading program was applied, so the drift of the tip of beam increases as the loading cycle advances. The test protocol for this cyclic reverse loading is shown in Fig. 7 which is consisted of one cycle of $\pm 0.5\theta_p$, 2 cycles in each $\pm 2.0\theta_p$, $\pm 4.0\theta_p$ and other cycles in $\pm 6.0\theta_p$ until the failure.

θ_p is the rotation corresponding to plastic moment capacity of bare steel beam (M_p), which is obtained by dividing beam's plastic moment by its initial stiffness. θ_b is the beam rotation angle based on definition presented in Fig. 8 and Eq. (5). Failure was defined as the fracture occurrence or 10% degradation from actual maximum strength obtained during the loading test.

$$\theta_b = \frac{\delta}{h'} = \frac{v_1 - \theta_c . h' - v_c}{h'} \quad [rad] \tag{5}$$

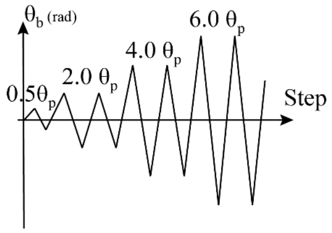

Fig. 7 Cyclic loading protocol

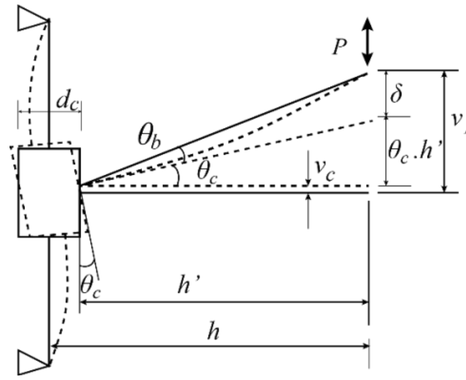

Fig. 8 Definition of beam rotation

3. Test results

3.1 M_b-θ_b Hysteresis Diagrams

M_b-θ_b hysteresis graphs are shown in Fig. 9. In these graphs M_b represents beam moment at column face and θ_b is beam rotation angle. It was observed that in the specimen which was connected to the RHS column with large width-to-thickness ratio of 29 (CB-29) rotation angle of composite beam reached to $2.0\theta_p$, while bare steel beam specimen with same width-to-thickness ratio (BS-29) reached to second cycle of $4.0\theta_p$. In the composite specimen which was connected to the smaller width-to-thickness ratio column (CB-22), considerable improvement of beam rotation capacity was observed and beam rotation angle could reach to $6.0\theta_p$. However, local buckling occurred in the beam bottom flange of this specimen.

3.2 Steel beam damage observations

3.2.1 Crack initiation and progress

In all specimens, regardless of width-to-thickness ratio and existence of slab, crack initiation happened at the root of weld access hole. However in the composite specimen with large width-to-thickness ratio of 29 (CB-29) this crack occurred in the considerable early cycle of loading, which was second cycle of $+2.0\theta_p$. While in the composite specimen with smaller width-to-thickness ratio of 22 (CB-22) this crack occurred in the later stage of loading, which was second cycle of $+4.0\theta_p$. Stage of loading which the crack initiated in the bare steel beam specimen (BS-29) was first cycle of $+4.0\theta_p$, which was later than CB-29 and earlier than CB-22. Crack initiation was defined when 0.2 mm crack was observed using crack scale. In Fig. 10 typical crack initiation and progress at the root of weld access hole is shown for all specimens in the first cycle of $+4.0\theta_p$. Fig. 11 shows that in which loading cycle first crack initiation was observed.

3.2.2 Final failure mode

Final failure of all specimens was determined by progress of above mentioned crack at the root of scallop of beam bottom flange, shown in Fig. 12. These fractures reproduced the failure modes of connections in the 1995 Hyogo ken-Nambu (Kobe) earthquake (AIJ 1995d 1995). Final failure manner of all specimens, were determined by quite ductile manner.

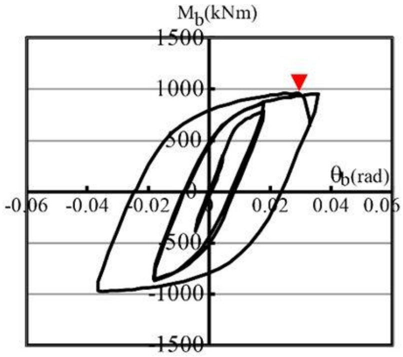

(a) BS-29

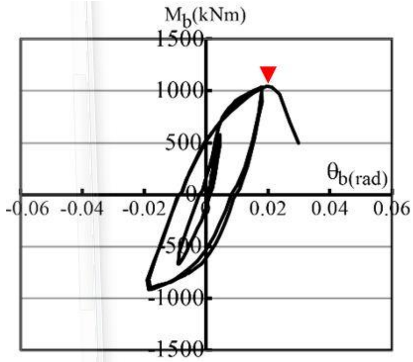

(b) BC-29

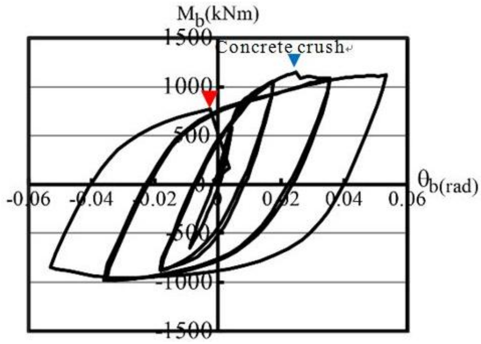

(c) BC-22

Fig. 9 M_b-θ_b hysteresis graphs

(a) BS-29: Crack initiation at $+3.0\theta_p$

(b) CB-29: Crack progress with width of 0.9 mm

(c) CB-22: No crack

Fig. 10 Typical crack initiation and progress at the root of weld access in the first cycle of $+4.0\theta_p$

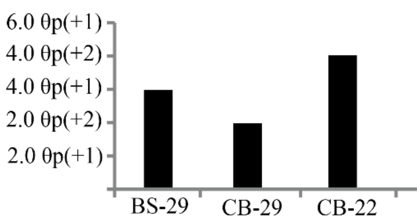

Fig. 11 First crack initiation during loading test

Fig. 12 Typical final failure mode

3.3 Concrete slab damage observations

The concrete slabs were subjected to subsequent tensile and compressive load and the formation of cracks traced as loading progressed. In both composite specimens, three patterns of slab damage were observed during the test. “Longitudinal crack” which was parallel to the steel beam, “transverse crack” which formed perpendicular to the steel beam, and “bearing crush” which occurred due to direct compression and formed at the vicinity of RHS column face.

As shown in Figs. 13(a) and (b), in both width-to-thickness ratios of 29 and 22 specimens, comparable transverse cracks and longitudinal cracks occurred at similar cycle of loading which was first cycle -0.5θ_p and +2.0θ_p, respectively.

Initiation of bearing crush at the corners of RHS column were also happened at similar cycle of loading which was first cycle of +2.0θ_p in both composite specimens, shown in Figs. 14 and 15. However, in CB-29 specimen this damage did not progressed due to failure of specimen, while for the specimen with smaller width-to-thickness ratio (CB-22), by progress of loading cycles, severe concrete crush occurred at the vicinity of column face and over whole slab depth during the first cycle of +4.0θ_p, shown in Fig. 16(b). This crush resulted in the sudden strength degradation which can be seen in the hysteresis diagram, shown in Fig. 9(c) of Section 3.1.

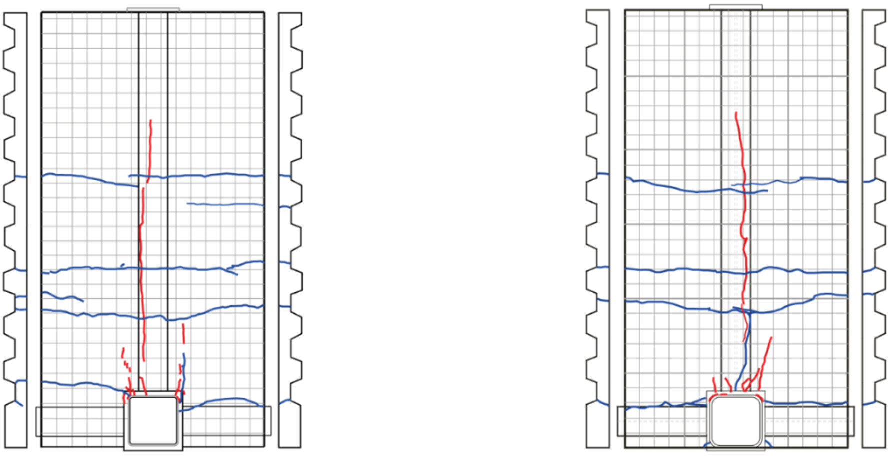

(a) CB-29 Specimen (b) CB-22 Specimen

Fig. 13 Formation of longitudinal and transverse cracks until end of first cycle of +2.0θ_p

(a) CB-29 (b) CB-22

Fig. 14 Initiation of bearing crush at corners of RHS column, comparable loading cycle $+2.0\theta_p(+1)$

(a) CB-29 (b) CB-22

Fig. 15 Comparable development of bearing crush until end of loading cycle $+2.0\theta_p(+2)$

(a) CB-29 (b) CB-22

Fig. 16 Final condition of concrete crush adjacent to the RHS column face

4. Effects of width-to-thickness ratio of RHS column

4.1 M_b-θ_b skeleton curves

The skeleton curves obtained from M_b-θ_b hysteresis diagrams are plotted in Figs. 17 (a) and (b). The method for plotting the skeleton curves, is shown in Fig. 18(a).

Fig. 17(a) corresponds to skeleton curve obtained from positive loading, and Fig. 17(b) corresponds to skeleton curve obtained from negative loading. In these graphs, actual plastic strength values are shown with solid circles, which are corresponding to one-sixth stiffness reduction, obtained by definition shown in Fig. 18(b).

According to Fig. 17, in positive flexure regardless of difference in column width-to-thickness ratio (B/t), considerable increase in the elastic stiffness of composite specimens can be seen. The elastic stiffness of CB-29 and CB-22 are 1.93 and 1.83 times of bare steel beam, respectively. However, in the case of negative flexure regardless of existence of slab, from the early stages of elastic region the stiffness is almost same.

Figs. 19(a) and (b) illustrate the amount of elastic stiffness of specimens in the positive and negative flexure, respectively. In the figure, the amount of elastic stiffness in $\pm0.5\theta_p$ and $\pm2.0\theta_p$

(second cycle) are shown, and the calculated stiffness is plotted with horizontal dotted line. In $+0.5\theta_p$ positive flexure, considerable increase of stiffness in both composite specimens compared with the bare steel beam specimen (BS-29) can be seen, however by progress of loading and development of damages in the concrete slab until $+2.0\theta_p(+2)$, stiffness of both composite beam specimens reduced, and finally reached to almost bare steel beam stiffness.

As shown in Fig. 19(b), in the negative flexure considerable difference for reduction of stiffness was not found between specimens. It can be explained that this behavior is resulted from removal of composite action in the negative flexure.

Regarding the actual plastic strength, from Fig. 17(a) it can be seen that in the positive flexure both composite specimens showed almost similar increase of plastic strength compared with BS-29. The plastic strength of CB-29 and CB-22 are 1.27 and 1.31 times of bare steel beam, respectively. Also it is shown that in the bare steel beam specimen BS-29, after reaching to actual plastic strength, almost steady increase of strength can be seen until 0.05 rad. After reaching to this rotation angle, strength degradation happened due to development of crack in the root of weld access hole (scallop), which was explained in Section 3.2.2. In the case of composite beam specimens, it can be seen that both specimens showed similar behavior until 0.018 rad., however in CB-29 specimen degradation of strength gradually happened due to initiation and progress of crack at the root of bottom flange weld access hole (scallop). On the other hand, in CB-22 specimen increase of strength continued by progress of loading until 0.025 rad., sudden strength

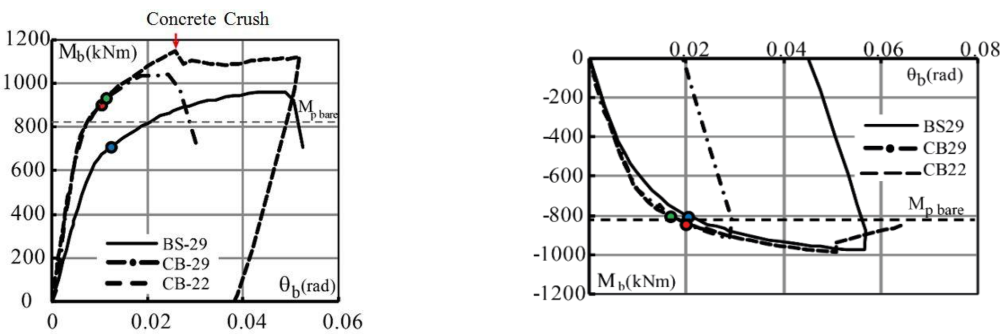

(a) Positive flexure (b) Negative flexure

Fig. 17 M_b-θ_b Skeleton curves

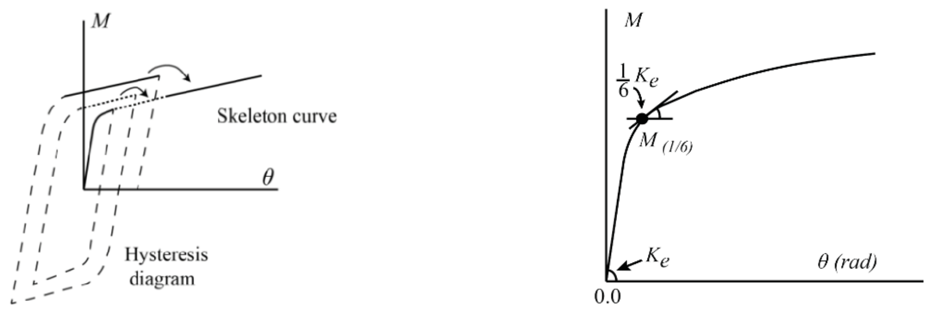

(a) Method for plotting the skeleton curve (b) Definition of strength

Fig. 18 Method for plotting the skeleton curve and definition of actual plastic strength

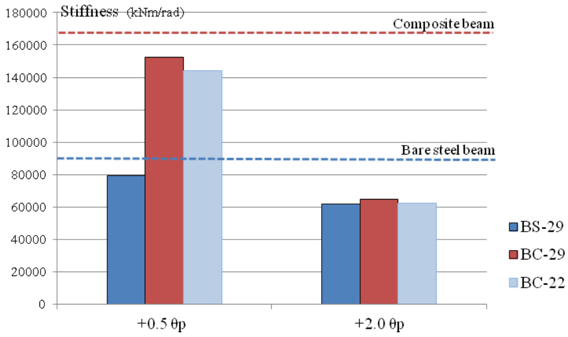

(a) Positive flexure

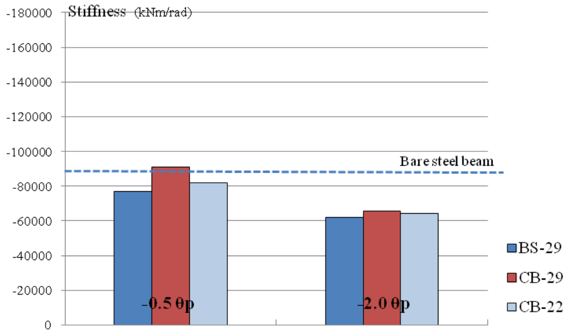

(b) Negative flexure

Fig. 19 Elastic stiffness of specimens

Table 4 Test results

Specimen	Plastic moment (kNm)		Ultimate flexural capacity (kNm)	
	M_{p+}	M_{p}-	$M_{\max+}$	$M_{\max}$-
BS-29	711	803	961	974
CB-29	903	842	1042	922
CB-22	934	801	1145	986

degradation can be seen in the skeleton curve of this specimen which was associated with concrete bearing crush at the vicinity of RHS column, which was discussed in Section 3.3.3, and resulted in 5% strength reduction. After this drop in the strength, constant moment transmitted until 0.05 rad.

Fig. 17(b) shows that in the negative flexure, actual plastic strength of all specimens were comparable to the calculated plastic moment capacity of bare steel beam, which is plotted with dotted horizontal line in the Figure.

Table 4 summarizes the results of observed ultimate strength of each specimen. Due to composite action, 8% increase in the ultimate flexural capacity of CB-29 observed compared with bare steel beam specimen BS-29. Reduction of RHS column width-to-thickness ratio in CB-22 resulted in 10% increase in the ultimate strength of this specimen compared with CB-29.

4.2 Strain behavior

Fig. 20 depicts the strain distribution across the length of beams top and bottom flange in the first cycle of $+2.0\theta_p$. Horizontal axis is the length and vertical axis is the amount of strain, measured by gauges attached at the 30 mm position from column face. As shown in Figs. 21(a), (b) and (c) in each specimen, strain of flanges was measured by the strain gauges which were mounted on the steel sections. Strain gauges were attached to the inside of top flange and both sides of bottom flange.

According to Fig. 20(a), it is found that the strain on the top flange of both composite specimens remained almost zero, while in the bare steel beam specimen BS-29, top flange strain amount reached to 2.7% negative strain. This behavior is resulted from the existence of slab, which provides constraint condition for the top flange of composite specimens.

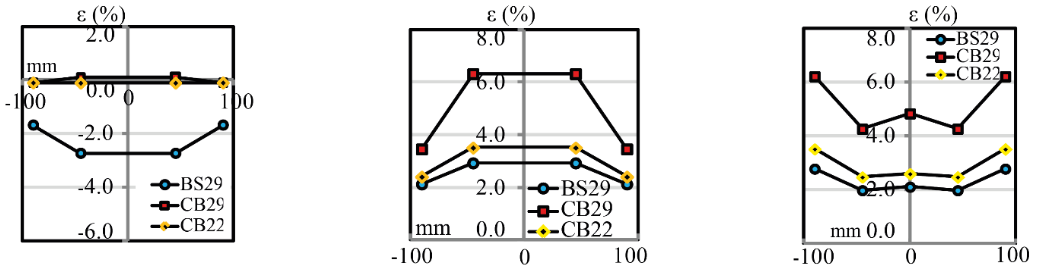

(a) Upper flange inside (b) Lower flange inside (c) Lower flange outside

Fig. 20 Strain distribution across the length of beams flange

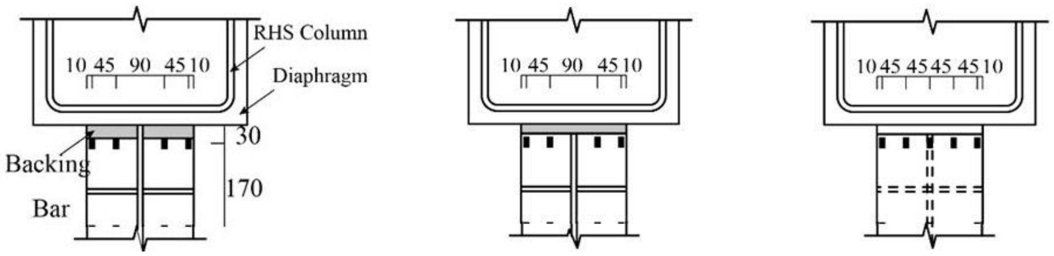

(a) Upper flange inside (b) Lower flange inside (c) Lower flange outside

Fig. 21 Strain gauges arrangement on the steel beam

Furthermore, for the bottom flange it can be seen that flanges were subjected to positive strain. In both sides of bottom flange of composite beam which was connected to the RHS column with large width-to-thickness ratio of 29 (CB-29 specimen), amount of strain is 2.2 times of bare steel beam specimen with same width-to-thickness ratio (BS-29). The amount of strain inside the bottom flange is higher than outside, in the center of flange. By reduction of RHS column width-to-thickness ratio in CB-22 specimen, 55% reduction of strain compared with CB-29 can be seen in both sides of flange. The amount of strain in CB-22 is just 1.2 times more than bare steel beam BS-29.

The above strain condition is associated with the specific loading cycle of $+2.0\theta_p$. The strain versus beam rotation angle is illustrated in Fig. 22. It is shown that during the entire loading stages, for all specimens regardless of existence of slab or difference of width-to-thickness ratios, by the progress of loading and increase of beam rotation angle, the amount of strain in the flanges increased. However, top flange of composite specimens sustained considerable smaller amount of strain, compared with bare steel beam specimen BS-29. On the other hand for the bottom flanges, although in the bare specimen BS-29 the strain condition was comparable with its top flange, however considerable increase of strain happened in both composite specimens CB-29 and CB-22.

It is also found that in the composite beam specimen with smaller width-to-thickness ratio CB-22, after the beam rotation angle reached to 0.025 *rad* and severe concrete crush occurred, sudden reduction in the slope of strain curve happened in the bottom flange. At the same time, slope of strain curve in the top flange increased. This behavior can be explained that following to severe concrete bearing crush in CB-22, reduction of top flange constraint condition occurred, and this resulted to change in the slope of strain curves of flanges.

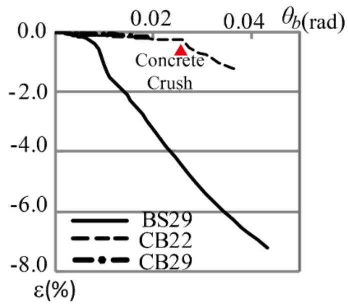

(a) Upper flange

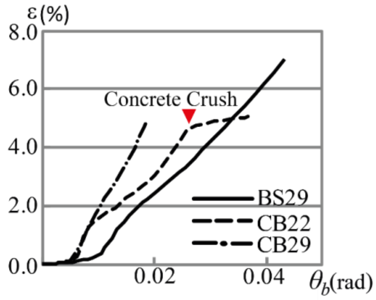

(b) Lower flange

Fig. 22 Strain versus beam rotation θ_b

According to strain behavior study and damage observations which were explained in Section 3.3.2, it is found that strain condition of bottom flange affected the crack growth and progress in each specimen, and finally this resulted in different rotation capacity of beams. In CB-29 specimen, higher amount of strain proceeded to earlier initiation and faster progress of crack compared with bare steel beam BS-29. In CB-22 specimen, despite the higher amount of bottom flange strain compared with BS-29, however after the occurrence of concrete bearing crash, reduction of strain in the bottom flange resulted in later initiation of crack at the root of weld access hole (scallop).

Fig. 23 depicts the crack growth in each specimen. Crack growth was investigated by plotting the measured crack opening (δ_{cr}) versus beam rotation. In this figure, η is the beam cumulative plastic rotation based on the definition shown on Fig. 24. Table 5 summarizes the results of cumulative rotation capacity of each specimen. Smaller amount of strain on the bottom flange of CB-22 resulted in later crack initiation, slower development and finally higher beam rotation capacity.

According to the design concept stipulated in the Japanese Recommendation for Design of Connections (AIJ 2012), ultimate strength of connection ${}_jM_u$, should be α times larger than plastic strength of connecting member M_p, represented by Eq. (6). In this concept, α is known as the connection factor

$${}_jM_u \geq \alpha.M_p \tag{6}$$

This concept is stipulated to ensure that connection failure to occur after sufficient plastic energy absorption in connecting member is achieved. Accordingly, the ultimate capacity of connection is to be evaluated.

In the case of bare beam-to-box column connection, beam plastic capacity is calculated as the product of section modulus Z_p, and yield strength σ_y, as

$$M_p = Z_p.\sigma_y \tag{7}$$

Ultimate flexural capacity of connection is composed of ultimate strength of flanges and web, represented by

$${}_jM_u = {}_jM_{fu} + {}_jM_{wu} \tag{8}$$

Flange ultimate flexural strength ${}_jM_{fu}$ is calculated as the product of flange section modulus, Z_{fp}`, and tensile stress of flange σ_{fu}

$$_{j}M_{fu} = Z_{fp}.\sigma_{fu} = A_f.d_b.\sigma_{fu} \tag{9}$$

To ensure a safe and convenient design in this type of connections, the evaluation of web moment capacity becomes the key issue. In the case of web connection, due to out-of-plane deformation, full capacity of web may not be achieved; so web ultimate flexural capacity $_{j}M_{wu}$ is represented as

$$_{j}M_{wu} = m_0.M_{wp} = m_0.Z_{wp}.\sigma_{wy} \tag{10}$$

where M_{wp} is web plastic capacity, Z_{wp} is web plastic modulus and σ_{wy} is web yield strength. m_0 is coefficient which is less than one for box column and equals to one for H-section column. The Parameter m_0 describes the reduction of web flexural capacity due to out-of-plane deformation. While m_0 is introduced in the AIJ (2012) for the bare beam-to-box column connection, there is no research for the introduction of m_0 for composite beam. Accordingly, connection factor α is introduced for bare beam-to-box column connection and there is no introduction of α for composite beam. Considering the fact that in the current structural design, composite beam ultimate capacity is assumed to be equal to the bare steel beam, importance of further study can be understood.

Fig. 25 illustrates the beam cumulative plastic rotation (η) versus connection factor (α) for this experimental test and also for specimens of Matsuo and Nakamura (1999) test results at Hiroshima University. Connection factor (α) is based on bare steel beam. In this Figure, black is representing the results of composite specimens and white is representing the results of bare steel beam specimens. Triangle is associated with Hiroshima University specimens and circle is associated with of this test specimens. Due to difference in materials between this test and Hiroshima test (SN400B), higher cumulative rotation capacity can be seen in the specimens of Hiroshima's experimental test, however it can be seen that in both tests for same connection factor (α) cumulative rotation of composite beam is reduced to almost less than half of bare steel beam. However, in current structural design in Japanese Recommendation for Design of Connections (AIJ 2012), rotation capacity of composite beam is supposed to be equal to the bare steel beam. These experimental test results describe the importance of further investigations for modification of connection factor α and clarification of stress transfer mechanism in the composite beam-to-RHS column connections.

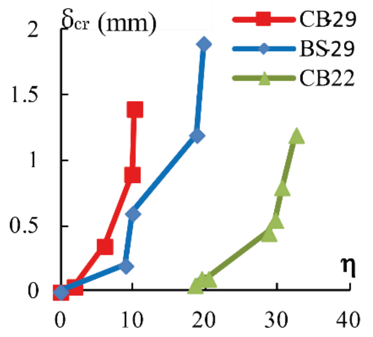

Fig. 23 Crack growth

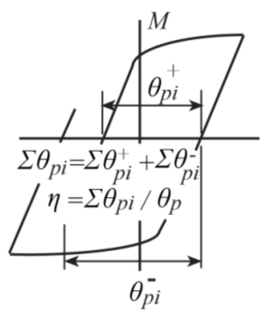

Fig. 24 Definition of "η"

Table 5 Cumulative rotation capacity

Specimen	η
BS-29	20.4
CB-29	10.7
CB-22	45.3

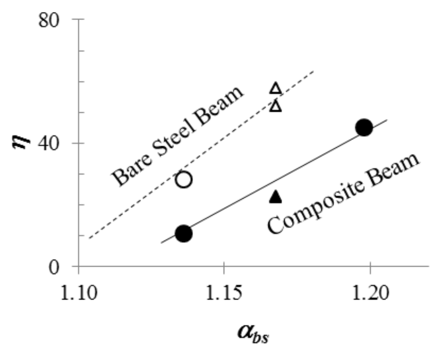

Fig. 25 Cumulative rotation capacity (η) versus connection factor (α) for this test and Hiroshima University specimens

5. Conclusions

This study was performed through the experimental tests on three full scale subassemblies to investigate the elasto-plastic behavior of composite beam connected to RHS columns with different width-to-thickness (B/t) ratios. Two composite connections are characterized by the same composite beam connected to columns having B/t ratio equal to 29 and 22, respectively. The cyclic response of such connections is compared to that of a bare steel connection whose RHS column has a B/t ratio equal to 29. The following conclusions are made:

- Test showed the importance of this parameter of RHS column, on the seismic behavior of composite beam. It was observed that reduction of RHS column width-to-thickness (B/t) ratio in composite specimens, did not result to considerable difference in the elastic stiffness and actual plastic strength of composite beams in the positive flexure, while considerable improvement in the cumulative rotation capacity was observed.
- Experimental test results revealed another specific difference between composite specimens. It was observed that in the specimen with smaller width-to-thickness (B/t) ratio, severe concrete bearing crush at the vicinity of column face resulted in the reduction in the rate of strain increase of bottom flange. This strain behavior, resulted in significant effect on the improvement of beam rotation capacity.
- Strain investigation showed that occurrence of concrete crush can be considered as the start of removal of composite action effect, and start of being close to the bare steel beam condition.
- According to considerable reduction of rotation capacity in composite beams connected to RHS column with large width-to-thickness (B/t) ratio of 29, observed in this test and published test data, and in order to prohibit strain concentration on the bottom flange, it is

recommended to avoid composite action in this *B*/*t* ratio. Application of slit between the column face and concrete slab is recommended in such condition.

- Considering the significant effect of concrete crush on the strain behavior of beam bottom flange, further investigation is needed to clarify the mechanical mechanism of stress transfer between slab, web and flanges, which FEA study will be presented in the next part of this research. The behavior of composite beam with slit will be studied in the next part of this research as well.

Acknowledgments

The research presented in this paper was supported by funds from the Ministry of Education of Japan (Monbukagakusho) which is truly acknowledged.

References

AIJ 1995d (1995), Performance of Steel Buildings during the 1995 Hyogoken-Nanbu Earthquake, Architectural Institute of Japan (AIJ), Japan, Tokyo.

AIJ (2010), Design Recommendations for Composite Constructions, Architectural Institute of Japan, Japan, pp. 63-79.

AIJ (2012), Recommendation for Design of Connections in Steel Structures; Architectural Institute of Japan, Japan, pp. 144-150.

AISC 341-10 (2010), *Seismic Provisions for Structural Steel Buildings*; American Institute of Steel Construction, Chicago, IL, USA.

AISC 360-10 (2010), *Specification for Structural Steel Buildings*; American Institute of Steel Construction, Chicago, IL, USA, pp. 16.1-xlviii.

Eslami, M. and Namba, H. (2013), "Ultimate flexural strength of composite beam connected to RHS column", *Architectural Institute of Japan* (*AIJ*) *Summaries of Technical Papers of Annual Meeting 2013*, Hokkaido, Japan, September, pp. 813-814.

Eslami, M. and Namba, H. (2014), "Effects of width-to-thickness ratio of RHS column on the elasto-plastic behavior of composite veam", *Memories of the Graduate Schools of Engineering and System Informatics Kobe University*, (Volume 6), pp. 1-6. DOI: 10.5047/gseku.e.2014.001

Eslami, M., Rahiminia, F. and Haghighi, B. (2009), "Experiences of design, fabrication and installation of TV towers with concrete shaft and head steel structures", *Proceedings of STESSA 2009 Behaviour of Steel Structures in Seismic Areas*, Bethlehem, PA, USA, August, pp. 79-86. DOI: 10.1201/9780203861592.ch12

Eslami, M., Namba, H. and Fukuoka, T. (2013), "Improvement of seismic behavior of composite beam connected to RHS column with application of slit and modification of studs layout", *Proceedings of the 10th Pacific Structural Steel* (*PSSC 2013*), Hokkaido, Japan, October, pp. 861-866. DOI: 10.3850/978-981-07-7137-9_200

FEMA-355E (2000), State of the Art Report on Past Performance of Steel Moment-Frame Buildings in Earthquakes; Federal Emergency Management Agency, Washington, D.C., USA, pp. C1-C24.

Fukuoka, T., Eslami, M. and Namba, H. (2013), "Plastic rotation capacity of composite beams connected to RHS columns: Part 1: Experimental tests using column with *D*/*t* = 29", *Architectural Institute of Japan* (*AIJ*) *Summaries of Technical Papers of Annual Meeting 2013*, Hokkaido, Japan, September, pp. 813-814.

JASS 6 (2007), Japanese Architectural Standard Specification JASS 6: *Structural Steelwork Specification for Building Construction*, Tokyo, Japan.

Kim, Y. and Oh, S. (2007), "Effect of the moment transfer efficiency of a beam web on deformation capacity at box column-to-H beam connections", *J. Construct. Steel Res.*, **63**(1), 24-36.

Matsuo, A. and Nakamura, Y. (1999), "A study on strain and plastic deformation capacity of composite beam-to-RHS column with thorough diaphragm (Part 1: Experimental planning and result)", *Proceedings of Annual Meeting of Architectural Institute of Japan* (*AIJ*), Tokyo, Japan, September, pp. 535-538.

Matsuo, A., Nakamura, Y., Takamatsu, T. and Matsui, Y. (2000), "Fracture and plastic deformation capacity of the welded joint of composite beam-to-steel column connections", *Proceedings of the 12th World Conference on Earthquake Engineering* (*WCEE*), Auckland, New Zealand, January-February, p. 0181.

Nakashima, M. and Chusilp, P. (2002), "A partial view of Japanese Post-Kobe seismic design and construction practices", *Earthq*. *Eng*. *Eng*. *Seismol*., **4**(1), 3-14.

Nakashima, M., Roeder, C.W. and Maruoka, Y. (2000), "Steel moment frames for earthquakes in United States and Japan", *J*. *Struct*. *Eng*., *ASCE*, **126**(8), 861-868.

Okada, K. and Yamada, S. (2001), "Experimental study on deformation capacity of composite beams with conventional type beam-to-column connections", *J*. *Struct*. *Constr*. *Eng*., *AIJ,* **547**, 161-168.

Okada, K., Sang-Hoon, T. and Yamada, S. (2004), "Tests on ductility capacity of composite beams", *Proceedings of the 7th Pacific Structural Steel Conference* (*PSSC*), Long Beach, CA, USA, March.

Saneei Nia, Z., Ghassemieh, M. and Mazroi, A. (2014), "Panel zone evaluation of direct connection to box column subjected to bidirectional loading", *The Structural Design of Tall and Special Buildings*, **23**(11), 833-853.

Tagawa Y., Nishiyama, I. and Yang, I. (2003), "Elasto-plastic behavior of new composite beam system", *Int*. *J*. *Steel Struct*., **3**(1), 45-52.

Tanaka, T., Suita, K. and Asakura, N. (2013), "Cyclic loading tests on composite beams with scallops (Part 15)," *Proceedings of Annual Meeting of Architectural Institute of Japan* (*AIJ*), Hokkaido, Japan, September, pp. 745-746.

Wang, W., Fang, C., Qin, X., Chen, Y. and Li, L. (2016), "Performance of practical beam-to-SHS column connections against progressive collapse", *Eng*. *Struct*., **106**, 332-347.

Yamada, S., Satsukawa, K., Kishikik, S., Shimada, Y., Matsuoka, Y. and Suita, K. (2009), "Elasto-plastic behavior of panel zone in beam to external column connection with concrete slab", *J*. *Struct*. *Construct*. *Eng*. (*Transactions of AIJ*), **74**(644), 1841-1849.

Yu, Y., Chen, Z. and Wang, X. (2015), "Effect of column flange flexibility on WF-beam to rectangular CFT column connections", *J*. *Construct*. *Steel Res*., **106**, 184-197.

BU